Cellular Physiology and Biochemistry

Cell Physiol Biochem 2018;51:1193-1206
DOI: 10.1159/000495497
Published online: 24 November 2018
Accepted: 16 November 2018

Original Paper

Comparative Study of MSCA-1 and CD146 Isolated Periosteal Cell Subpopulations

Felix Umrath[a] Carla Thomalla[a] Simone Pöschel[b] Katja Schenke-Layland[b] Siegmar Reinert[a] Dorothea Alexander[a]

[a]Department of Oral and Maxillofacial Surgery of the University Hospital of Tübingen, Tübingen, [b]Department of Women's Health of the Eberhard-Karls University Tübingen, Tübingen, Germany

Key Words
Cranial periosteal cells • MSCA-1 • CD146 • Multispectral imaging flow cytometry • Cell sorting

Abstract
Background/Aims: Periosteal tissue is a valuable source of multipotent stem cells for bone tissue engineering. To characterize these cells in detail, we generated an immortalized human cranial periosteal cell line and observed an increased MSCA-1 and CD146 expression, as well as an earlier and stronger mineralization compared to the parental cells. Further, we detected a higher osteogenic potential of MSCA-1^{high} compared to MSCA-1^{low} cranial periosteal cell (CPC) fractions. In the present study, a possible synergism of MSCA-1 and CD146 for periosteal cell mineralization was investigated. ***Methods:*** MSCA-1/CD146 positive and negative CPCs were magnetically isolated (MACS) or sorted by flow cytometry (FACS) and subjected to osteogenic differentiation. The expression of osteogenic marker genes in the four subpopulations was analyzed by quantitative real-time PCR. Furthermore, the co-expression of osteogenic markers/antigens was analyzed by multispectral imaging flow cytometry (ImageStream, AMNIS). The mineralization potential was assessed by the quantification of alizarin stainings. ***Results:*** While the total cell yield after separation was higher using MACS compared to the FACS approach, the isolation of MSCA-1$^{+/-}$ and CD146$^{+/-}$ subpopulations was more efficient with the FACS separation. The accuracy of the FACS separation of the four distinguished cell subpopulations was confirmed by multispectral imaging flow cytometry. Further, we detected increasing levels of MSCA-1 and CD146 during *in vitro* differentiation in all subpopulations. However, MSCA-1 expression was significantly higher in the MSCA-1^{+}/CD146^{+} and MSCA-1^{+}/CD146^{-} subpopulations, while CD146 expression remained clearly lower in these fractions. Significantly higher gene expression levels of osteogenic markers, *ALP* and *RUNX2*, were detected in MSCA-1^{+} compared to MSCA-1^{-} CPCs at different time points during *in vitro* differentiation.Staining and quantification of calcium phosphate precipitates revealed a significantly higher mineralization potential of MACS separated MSCA-1^{+} and CD146^{-} CPCs, compared to their respective counterparts. FACS sorted CPCs displayed earlier mineralization in both MSCA-1^{+} fractions (d13), while later (d28) only the CD146^{+}/MSCA-1^{-} fraction had a significantly lower calcium phosphate concentration compared to all other fractions.

Dorothea Alexander-Friedrich

Dept. of Oral and Maxillofacial Surgery, University Hospital of Tübingen
Osianderstr. 2-8, 72076 Tübingen (Germany)
Tel. +49/70712982418, E-Mail dorothea.alexander@med.uni-tuebingen.de

Conclusion: Our results demonstrate, that MSCA-1^{+} cells isolated from CPCs represent a subpopulation with a higher osteogenic potential. In contrast, we found a lower osteogenic potential in CD146^{+} CPCs. In conclusion, only MSCA-1, but not CD146, is a suitable marker for the isolation of osteoprogenitors from CPCs.

Introduction

Periosteum, the thin membrane surrounding and nourishing the bones, contains osteoprogenitor cells in the inner layer, which can form new bone tissues. It's properties and the potential of periosteum derived mesenchymal stromal cells (MSCs) in bone tissue engineering has been reviewed in detail by Ferretti and Mattioli-Belmonte [1]. In the field of oral and maxillofacial surgery, especially oral and cranial periosteal cells are a promising source for new cell based bone reconstruction therapies, and therefore need to be characterized in detail [2].

To increase the quality of patient derived periosteal MSCs, markers for the isolation of pure osteoprogenitor cells need to be identified.

Previously, we demonstrated that the MSCA-1-enriched subpopulation from the human jaw periosteal tissue exhibits higher osteogenic potential compared to the MSCA-1^{low} cell fraction [3]. Furthermore, we generated an immortalized cell line derived from the human cranial periosteum and analyzed its features in comparison with the primary cells from which the cell line was derived [4]. Due to the different origin and significantly higher CD146 (MUC-18, MCAM) surface expression by the SV40 T antigen immortalized cranial periosteal cells, we aimed to analyze the osteogenic potential of the MSCA-1$^{+/-}$ and CD146$^{+/-}$ subpopulations isolated from this cell line in the present study.

Multipotent mesenchymal stromal cells (MSCs) are identified by the cell surface expression of the following markers: CD73, CD90 or CD105 [5, 6]. MSCA-1 was described to coincide with the tissue non-specific alkaline phosphatase (TNAP) [7] and to be expressed by MSCs from different tissues [3, 8-12].

Patients with TNAP deficiency suffer from bone abnormalities caused by hypomineralization [13, 14]. TNAP hydrolyzes inorganic pyrophosphates, which normally inhibit calcium phosphate formation within the extracellular matrix [15]. Based on two different promoter regions, tissue-related differences in alkaline phosphatase exist in the bones, liver and kidneys [16]. In addition to its role in bone development, TNAP exerts several other functions in liver/kidney, promotes vessel calcification, and plays a role in the neuron/brain development, as reviewed in the recent study by Esteve and co-authors [17].

Pericytes stabilize microvessels and play an important role in the regeneration of vascularized tissues and instructing extravasating leucocytes towards their target by motility programs [18]. A perivascular origin of multipotent MSCs isolated from different human tissues has been hypothesized [19]. CD146 is also described as highly expressed in human bone marrow stromal cells (also known as mesenchymal stem cells), which generate osteogenic cells among other cell lineages. *In situ*, osteoblasts and bone-lining cells do not express CD146 [20].

According to our experience, jaw and cranial periosteal cells are normally CD146 negative. The primary cranial periosteal cells, creating the parental cells to the immortalized cell line used in the present work, showed a low CD146 expression. However, the resulting immortalized cells were 70-80% CD146 positive, as previously described [4].

The goal of this study was to determine whether the high CD146 surface expression of immortalized periosteal cells (TAg cells) correlates with the high mineralization capacity as compared to the primary cells from which they derive. Furthermore, we also compared the osteogenic potential of isolated MSCA-1$^{+/-}$ and CD146$^{+/-}$ subpopulations in the present study.

Materials and Methods

Cell isolation and culture

As previously described [4], we generated a human SV40 T-antigen immortalized cranial periosteal cell line, referred to as TAg cells in this article. The work with the cells included in this paper was approved by the local ethics committee (approval number 534/2013BO1) and carried out after written consent of the patient.

TAg cells were cultured in DMEM/F-12 (Thermo Fisher Scientific, Waltham, Massachusetts, USA) containing 10% FCS (Sigma-Aldrich, Steinheim, Germany), 1% amphotericin B (Biochrom, Berlin, Germany) and penicillin/streptomycin (Lonza, Basel, Switzerland) in the presence of 0.25 mg/ml G418 (immortalization maintenance dose). DMEM-cultured cells were passaged using trypsin-versene (1x, Lonza, Basel, Switzerland) every three or four days.

Magnetic separation of the MSCA-1$^{+/-}$ and CD146$^{+/-}$ cell subpopulations

The entire TAg periosteal cell population was subjected to magnetic separation to isolate the MSCA-1$^{+/-}$ and CD146$^{+/-}$ cell fractions as previously described [21]. In brief, TAg cells were incubated with the FcR blocking reagent and anti-MSCA-1/-CD146 MicroBeads (Miltenyi Biotec, Bergisch Gladbach, Germany) for 20 min at 4°C. After washing, the samples were applied to pre-separation filters and then onto MS columns. The MSCA-1^{+}/CD146^{+} cells remained within the columns in the magnetic field. After removing the columns from the magnetic field, positive fractions could be eluted.

Separation of the MSCA-1$^{+/-}$/CD146$^{+/-}$ cell subpopulations by FACS

The TAg cells were subjected to fluorescence-activated cell sorting (FACS) to isolate four distinct fractions: P1: CD146^{+}/MSCA-1^{-}, P2: CD146^{+}/MSCA-1^{+}, P3: CD146^{-}/MSCA-1^{-} and P4: CD146^{-}/MSCA-1^{+}. TAg cells were double-stained with specific anti-MSCA-1-PE and anti-CD146-APC antibodies, and separated into four fractions by fluorescence activated cell sorting (FACS), according to the gates shown in Fig. 1.

Cells were harvested using trypsin-versene (1x, Lonza, Basel, Switzerland) and incubated on ice for 15 min in 20 µl/10^6 blocking buffer (PBS, 0.1% BSA, 10% Gamunex (human immune globulin solution, Talecris Biotherapeutics GmbH, Frankfurt, Germany)). 50 µl/10^6 cells FACS-buffer (PBS, 0.1% BSA), 10 µl/10^6 cells anti-MSCA-1-PE antibody (Miltenyi Biotec, Bergisch Gladbach, Germany) and 5 µl/10^6 cells anti-CD146-APC (Miltenyi Biotec) were added und incubated on ice for 20 min. Cells were washed twice with 1 ml/10^6 cells FACS-buffer, suspended in 50 µl/10^6 cells PBS and transferred into 5 ml FACS-tubes. Sorting was performed

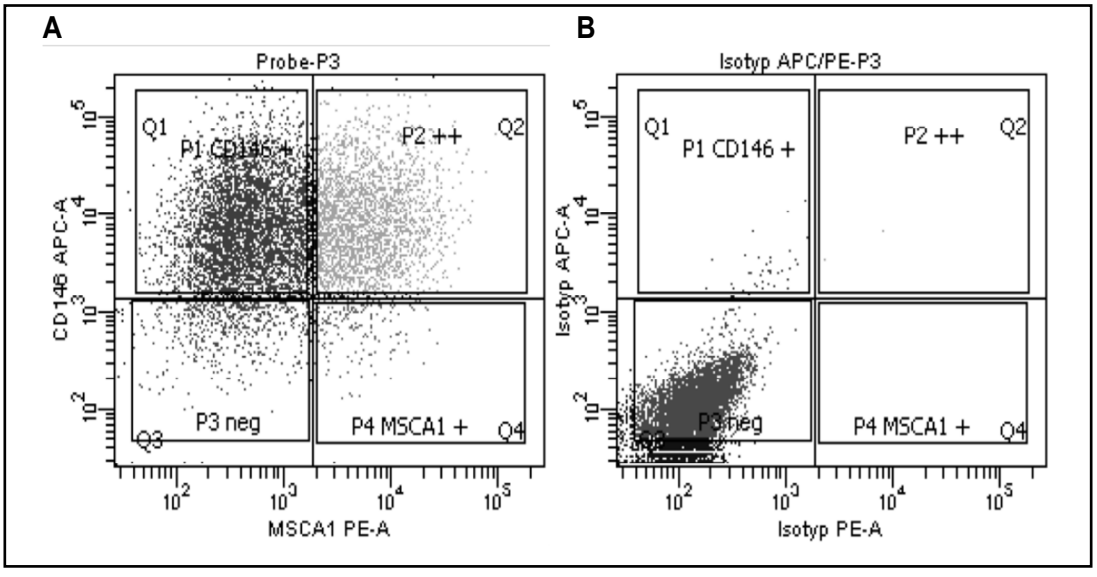

Fig. 1. Representative dot blots and gating strategy for the separation of MSCA-1$^{+/-}$/CD146$^{+/-}$ subpopulations by FACS. A) anti-MSCA-1-PE and anti-CD146-APC stained sample B) anti-IgG1-PE and anti-IgG1-APC stained isotype control.

with a FACSaria I cell sorter (BD Biosciences, Franklin Lakes, USA) using FACSDiva software version 6.1.3. Gates were set on the basis of IgG1-PE (R&D Systems, Inc., Minneapolis, USA) and IgG1-APC (BioLegend, San Diego, USA) isotype controls, which were prepared in parallel. Sorted cells were collected in 5 ml FACS-tubes containing 1 ml DMEM/F12 containing 50% FBS.

Table 1. Antibodies used for FACS and imaging flow cytometry

Antigen	Isotype	Conjugate	Company	Product-No.
MSCA-1	mouse IgG1	PE	MACS Miltenyi	130-093-587
CD146	mouse IgG1	APC	MACS Miltenyi	130-097-942
OCN	mouse IgG1	AlexaFluor 488	R&D Systems	IC1419G
RUNX2	mouse IgG2a	-	Abcam	ab76956
ALPL	mouse IgG1	-	R&D Systems	MAB1448
mouse IgG1	goat polyclonal Ig	DyLight 405	BioLegend	409109
mouse IgG2	rat IgG	PE-Cy7	BioLegend	407114
-	mouse IgG1	APC	BioLegend	400122
-	mouse IgG1	PE	R&D Systems	IC002P

Osteogenic differentiation of sorted TAg cell fractions

Following FACS sorting, separated TAg cell fractions (P1-P4) were seeded into 6 well plates at a density of $3 \cdot 10^4$ cell/well (n = 3 independent samples for each cell subpopulation). Three days later, osteogenic induction was initiated using an osteogenic medium (Ob - DMEM/F12 containing 10% FCS, 10 mM β-glycerophosphate, 100 µM L-ascorbic acid 2-phosphate and 4 µM dexamethasone, Sigma-Aldrich), and medium was changed every other day. Control samples (undifferentiated) were cultured in DMEM/F12 containing 10% FCS (Co). Osteogenic differentiation was carried out for 13, 20 and 28 days before cells were fixed and stained using Alizarin S. Cells were analyzed by imaging flow cytometry after 2, 5 and 10 days of osteogenic differentiation. Gene expression analysis was carried out after 2, 5, and 10 days of osteogenic differentiation.

Multispectral imaging flow cytometry analysis of sorted MSCA-1$^{+/-}$/CD146$^{+/-}$ cell fractions

Following osteogenic differentiation for 2, 5 and 10 days, cells were harvested from the culture plates using trypsin-versene (1x, Lonza, Basel, Switzerland). From each fraction and culture condition, cells of three independent wells were pooled and blocked with 10% Gamunex for 15 min. Surface antigens MSCA-1 and CD146 were labeled with specific mouse anti-human anti-CD146-APC and anti-MSCA-1-PE antibodies (Miltenyi Biotec), as previously described. For intracellular staining, cells were permeabilized by incubation with fixation/permeabilization solution (BD Biosciences) for 20 min and washed with BD Perm/Wash™ buffer (BD Biosciences, Franklin Lakes, USA). To prevent unspecific binding intracellular staining was carried out in 50 µl BD Perm/Wash™ buffer containing 10% Gamunex. Intracellular antigens were stained using directly labeled mouse anti-human anti-OCN-AlexaFluor488 (R&D Systems, Inc., Minneapolis, USA) and unlabeled mouse anti-human anti-RUNX2 (Abcam, Cambridge, UK) and mouse anti-human anti-ALPL (R&D Systems, Inc., Minneapolis, USA) primary antibodies. Primary antibodies were captured with goat anti-mouse anti-IgG1-DyLight405 and rat anti-mouse anti-IgG2-PE-Cy7 secondary antibodies (BioLegend, San Diego, USA). Cells incubated with PE-, APC- and AlexaFluor488-labeled isotype antibodies and DyLight405- and PE-Cy7-labeled secondary antibodies served as negative controls. All antibodies used for FACS and multispectral imaging flow cytometry are listed in Table 1. After staining, cells were resuspended in 50 µl BD Perm/Wash™ Buffer (BD Biosciences). Imaging flow cytometry was carried out with the ImageStream®X Mark II Imaging Flow Cytometer (Merck Millipore, Billerica, USA) using INSPIRE software. For data evaluation, IDEAS software version 6.0 was used.

Analyses of the osteogenic potential of MSCA-1$^{+/-}$/CD146$^{+/-}$ cell monolayers

TAg cells sorted using MACS and FACS (n = 3 independent samples for each cell subpopulation and experiment) were differentiated for 13, 20 and 28 days as described previously. Subsequently, the cell monolayers were fixed for 15 min at RT with 4% formalin. After washing with PBS, a pH 4.2, 40 mM Alizarin red dye solution was added and incubated for 30 min while shaking. Thereafter, cell monolayers were intensively washed with ddH_2O and visualized using an inverse microscope. For quantification, bound Alizarin red dye was dissolved using acetic acid, and cell monolayers were scraped off from the plates. Samples were heated at 85°C for 10 min, cooled down for 5 min on ice and centrifuged for 15 min at 20,

000 g. After neutralization with 10% ammonium hydroxide, samples were measured at 405 nm using a microplate reader (BioTek Instruments GmbH, Bad Friedrichshall, Germany), and calcium concentrations were calculated in relation to a standard curve (0.002-0.2 mM).

Gene expression analysis of sorted MSCA-1$^{+/-}$/CD146$^{+/-}$ cell fractions by quantitative PCR

Gene expression of FACS separated cell populations was performed after 2, 5 and 10 days of osteogenic differentiation with Ob-medium and compared to untreated cells (Co). RNA isolation from sorted TAg cells (n = 3 independent samples for each cell subpopulation) was carried out using the NucleoSpin RNA XS kit (Macherey-Nagel, Düren, Germany) following the manufacturer's instructions. The amount of isolated RNA was measured and quantified with a Qubit 3.0 fluorometer and the provided RNA HS Assay Kit (Thermo Fisher Scientific Inc., Waltham, USA). 0.5 µg of RNA was used for first-strand cDNA synthesis using the Advantage RT-for-PCR Kit (Clontech Laboratories, Mountain View, USA) following the manufacturer's instructions.

The quantification of mRNA expression levels was performed using the real-time LightCycler System (Roche Diagnostics, Mannheim, Germany). For the PCR reactions, commercial primer kits (Search LC, Heidelberg, Germany) and DNA Master Sybr Green I (Roche, Basel, Switzerland) were used. The amplification was performed following a touchdown PCR protocol of 40 cycles (annealing temperature between 68-58°C), following the manufacturer's instructions. The transcript levels were normalized to those of the housekeeping gene glycerinaldehyde 3-phosphate dehydrogenase (GAPDH), and illustrated as a ratio of the target versus housekeeping gene transcripts.

Statistical analysis

Statistical analyses were performed using the unpaired t-test. A p-value < 0.05 was considered statistically significant.

Results

Separation of MSCA-1 and CD146 labeled subpopulations by MACS and FACS

Efficiencies of MACS separations. The magnetic separations using the specific anti-MSCA-1 antibodies resulted in an average total cell yield of 62.65 ± 12.51%. Thereof, 86.64 ± 1.56% were MSCA-1-negative, and 13.36 ± 1.56 % were MSCA-1-positive, as shown in Table 2. The magnetic separations using the specific CD146 antibodies resulted in a very similar average total cell yield of 62.88 ± 11.69%. Thereof, 83.64% ± 6.68 were CD146$^-$, and 16.36% ± 6.68 were CD146$^+$, as shown in Table 3.

Efficiencies of FACS separations. FACS sorting (n = 5) resulted in an average total cell yield of 40.74 ± 8.76 % (Table 4), which is considerably lower than the cell yield after MACS separation (62.88 ± 11.69 %). The total number of sorted cells from the four subpopulations and the total cell yields (%) are given in Table 4. Fig. 2 illustrates the distribution of the four subpopulations after sorting, with CD146$^+$/MSCA-1$^-$ being the most abundant subpopulation (55.79 ± 7.81 %), and CD146$^-$/MSCA-1$^+$ being the rarest subpopulation (3.65 ± 0.85 %). The double positive subpopulation CD146$^+$/MSCA-1$^+$ and the double negative subpopulation CD146$^-$/MSCA-1$^-$ were represented with 29.84 ± 7.81 %, and 10.72 ± 2.83 % respectively. We detected clear differences in terms of separation efficiencies between MACS and FACS separation. While the percentage of MSCA-1$^+$ and CD146$^+$ cells using MACS separation averaged 13.4 ± 1.56 % and 16.36 ± 6.68 % respectively, MSCA-1$^+$ and CD146$^+$ fractions separated by FACS were significantly higher with 33.49 ± 8.39 % and 85.63 ± 3.15 % respectively. These results indicate a very low accuracy of the MACS separation, especially for CD146.

Table 2. Overview of the performed magnetic separations (n = 4) using the anti-MSCA-1 antibodies. Total cell numbers and their percentages before and after separations

Cell numbers before separation	Total number of MSCA-1$^+$ cells	Total number of MSCA-1$^-$ cells	Total cell yield (%)	Amount of cells (%) MSCA-1$^+$	MSCA-1$^-$
1. 1.23E+08	6.94E+06	5.11E+07	47.30	11.96	88.04
2. 1.54E+08	1.38E+07	7.49E+07	57.60	15.57	84.43
3. 6.75E+07	6.52E+06	4.29E+07	73.21	13.19	86.81
4. 9.71E+07	8.96E+06	6.14E+07	72.50	12.73	87.27
Average cell yield and amount of MSCA-1$^{+/-}$ cells			62.65±12.51	13.4±1.56	86.64±1.56

Table 3. Overview of the performed magnetic separations (n = 4) using the anti-CD146 antibodies. Total cell numbers and their percentages before and after separations

Cell numbers before separation	Total number of separated CD146$^+$ cells	CD146$^-$ cells	Total cell yield (%)	Amount of cells (%) CD146$^+$	CD146$^-$
1. 1.15E+08	1.82E+07	5.66E+07	64.90	24.35	75.65
2. 1.04E+08	4.70E+06	4.38E+07	46.59	9.69	90.31
3. 1.13E+08	1.03E+07	7.41E+07	74.43	12.20	87.80
4. 9.99E+07	1.26E+07	5.30E+07	65.62	19.22	80.78
Average cell yield and amount of CD146$^{+/-}$ cells			62.88±11.69	16.36±6.68	83.64±6.68

Table 4. Overview of the performed FACS sorting (n = 5) using both anti-MSCA-1 and anti-CD146 antibodies. Total cell numbers before FACS separation, number of cells separated, and percentage of cells recovered after sorting

Cell numbers before separation	Total number of separated cells MSCA-1$^-$/CD146$^+$	MSCA-1$^+$/CD146$^+$	MSCA-1$^-$/CD146$^-$	MSCA-1$^+$/CD146$^-$	Total cell yield (%)
1. 6.10E+07	1.45E+07	6.29E+06	2.43E+06	7.53E+05	39.31
2. 7.50E+07	1.28E+07	7.65E+06	2.45E+06	1.06E+06	31.99
3. 6.00E+07	1.36E+07	4.12E+06	1.66E+06	3.65E+05	32.97
4. 3.80E+07	9.86E+06	4.39E+06	1.62E+06	5.51E+05	43.21
5. 3.31E+07	1.07E+07	4.00E+06	3.19E+06	6.71E+05	56.20
Average total cell yield					40.74±8.76

Osteogenic potential of MACS separated TAg cells

Fig. 3 illustrates the Alizarin red staining for the visualization of calcium phosphate precipitates formed within the monolayers of the four magnetically isolated cell fractions after 20 days of osteogenic differentiation (upper panel). The osteogenic pattern of the MSCA-1$^{+/-}$ fractions was as expected, and previously observed in the primary cells from which the TAg cells were derived. MSCA-1$^+$ TAg cells showed a higher mineralization degree in comparison with the MSCA-1$^-$ cells. Surprisingly, the CD146 isolated cell fractions showed an opposite pattern. CD146$^-$ TAg cells showed a higher mineralization potential than the CD146$^+$ cells. The mineralization pattern representatively visualized in Fig. 3 was confirmed by exact quantification of the Alizarin dye bound to the four analyzed TAg cell monolayers after osteogenic induction, as illustrated in the lower panel of Fig. 3.

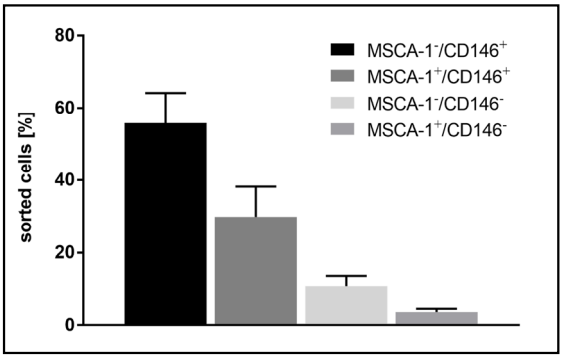

Fig. 2. Average distribution (%) of MSCA-1$^{+/-}$/CD146$^{+/-}$ subpopulations sorted by FACS (n=8).

Calcium concentrations did not differ significantly between the unstimulated controls of the MSCA$^{+/-}$ and CD146$^{+/-}$ fractions. However, we detected significantly higher calcium concentrations in osteogenically induced MSCA-1$^+$ (0.16 ± 0.03 mM versus the corresponding negative fraction with 0.07 ± 0.03 mM, $p < 0.01$) and CD146$^-$ TAg cells (0.10 ± 0.05 mM versus the corresponding positive fraction with 0.05 ± 0.03 mM, $p < 0.05$).

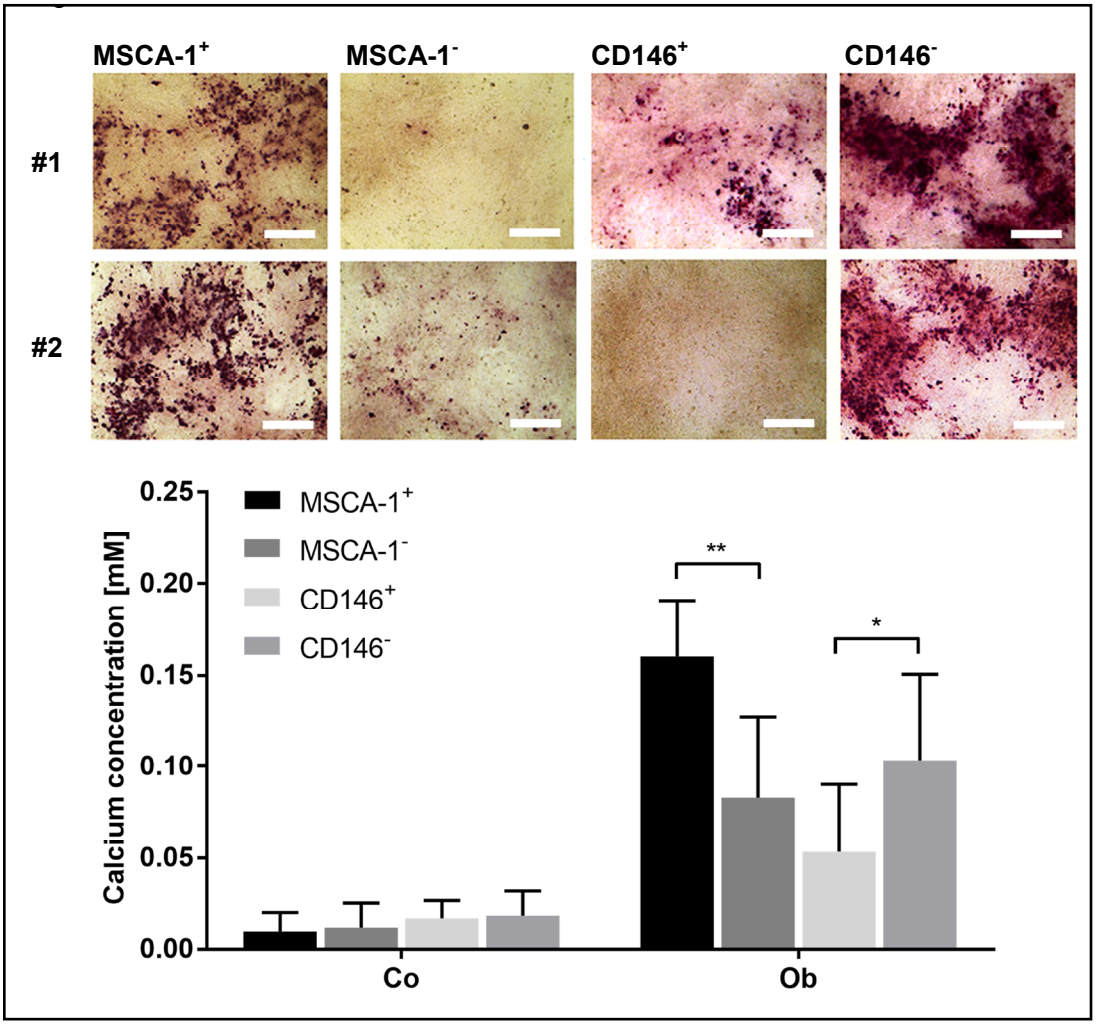

Fig. 3. Upper Panel: Staining of calcium phosphate precipitates formed by MACS separated MSCA-1$^{+/-}$ and CD146$^{+/-}$ fractions by Alizarin red after 20 days of osteogenic differentiation. Representative bright-field images (4x magnification) of differentiated MSCA-1$^{+/-}$ and CD146$^{+/-}$ TAg cells from two independent separations (#1 and #2). Scale bars equal 500 µm. A higher mineralization potential (precipitates stained red) was detected in MSCA-1^{+} and CD146^{-} TAg cells. Lower panel: Quantification of calcium precipitates in unstimulated and osteogenically differentiated MSCA-1$^{+/-}$ and CD146$^{+/-}$ TAg cells. Calcium concentrations (mM) were quantified after dissolving the Alizarin dye from the stained monolayers. Significantly higher calcium concentrations were detected in magnetically separated (A) CD146^{-} cell fractions (* $p<0.05$) and (B) MSCA-1^{+} (* $p<0.01$) of the entire TAg cell population. Co – unstimulated cells, Ob – osteogenically induced cells.

Osteogenic potential of FACS separated TAg cells

Fig. 4 illustrates the Alizarin red staining for the visualization of calcium phosphate precipitates formed within the monolayers of the four FACS separated subpopulations of TAg cells after 13 days of osteogenic differentiation (upper panel). As already observed after MACS separation, MSCA-1^{+} subpopulations showed a higher mineralization potential than MSCA-1^{-} subpopulations. Furthermore, the MSCA-1^{+}/CD146^{-} fraction showed clearly higher amounts of calcium phosphate precipitates than the double-positive MSCA-1^{+}/CD146^{+} fraction. This corresponds to the negative correlation of CD146 expression and mineralization, previously observed in MACS sorted CD146^{+} cell fractions. MSCA-1^{-}/CD146^{-} subpopulations showed little, and MSCA-1^{-}/CD146^{+} subpopulations showed little to no mineralization after 13 days of differentiation, which further supports the previous observation.

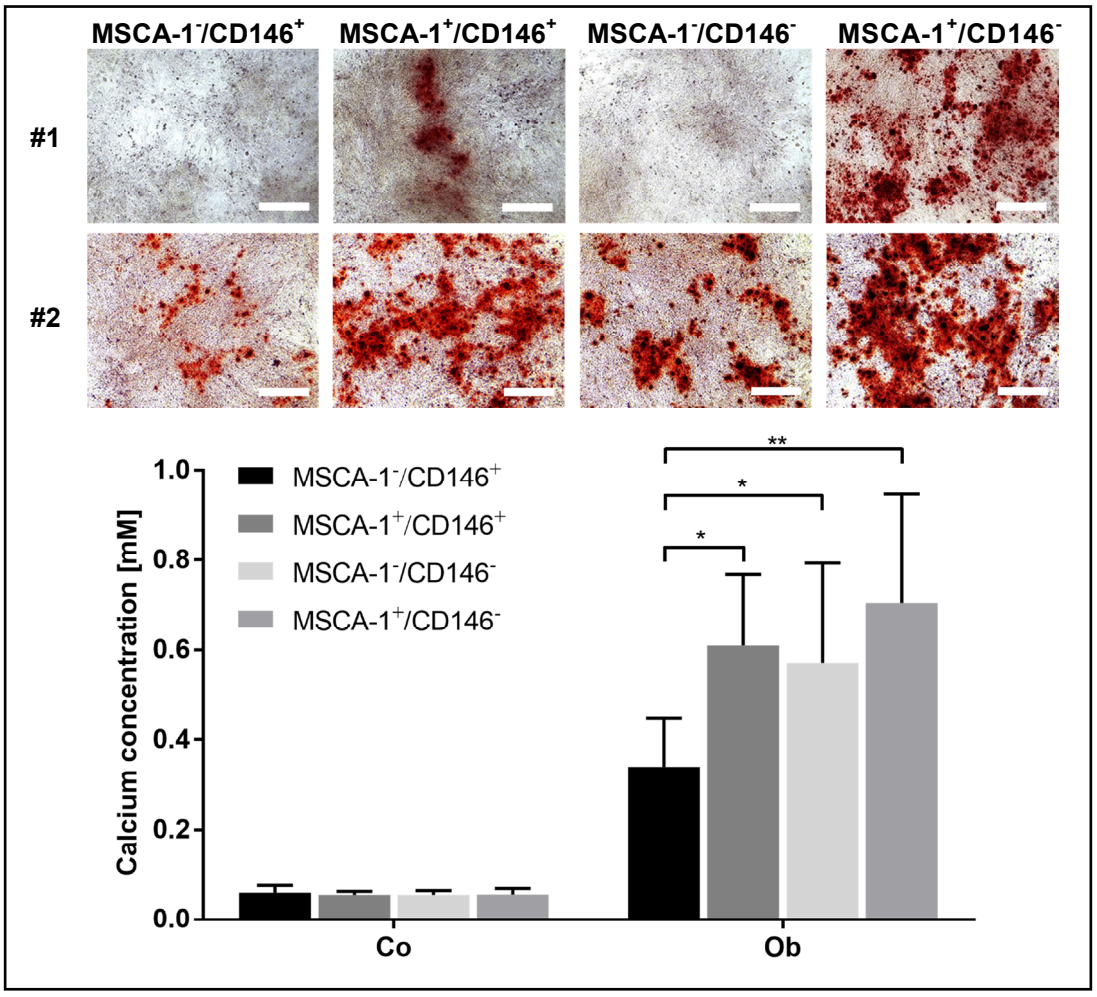

Fig. 4. Upper Panel: Staining of calcium phosphate precipitates formed by FACS separated MSCA-1$^{+/-}$/CD146$^{+/-}$ fractions by Alizarin red after 13 days of osteogenic differentiation. Representative bright-field images (4x magnification) of differentiated MSCA-1$^{+/-}$/CD146$^{+/-}$ TAg cells from two independent separations (#1 and #2). Scale bars equal 500 µm. Similarly, as observed in MACS sorted cell fractions (Fig. 3), a higher mineralization potential (precipitates stained red) was detected in MSCA-1^{+} and CD146^{-} TAg cell subpopulations. Lower panel: Quantification of calcium precipitates formed by FACS sorted MSCA-1$^{+/-}$/CD146$^{+/-}$ TAg cell subpopulations after 28 days of osteogenic differentiation. Calcium concentrations (mM) were quantified after dissolving the Alizarin dye from the stained monolayers. We detected significantly lower calcium concentrations (* $p<0.05$, ** $p<0.01$) in the MSCA-1^{-}/CD146^{+} fraction compared to all other fractions of the entire TAg cell population. Co – unstimulated cells, Ob – osteogenic induced cells.

For calcium quantification, the sorted TAg cells were incubated in osteogenic medium for 28 days (lower panel). While differences in the mineralization were clearly visible at day 13 (upper panel), strong mineralization was observed in all sorted cell fractions at day 28.

Calcium concentrations in Fig. 4 show similar tendencies as previously observed in MACS separated cell cultures (Fig. 3). As expected, we observed a higher mineralization potential of MSCA-1^{+} subpopulations compared to MSCA-1^{-} subpopulations. The highest calcium concentration was measured in the MSCA-1^{+}/CD146^{-} fraction (0.70 ± 0, 08 mM), followed by the double positive (MSCA-1^{+}/CD146^{+}, 0.61 ± 0.05 mM) and the double negative (MSCA-1^{-}/CD146^{-}, 0.57 ± 0.07 mM) fraction. Significantly lower calcium concentrations were detected in the MSCA-1^{-}/CD146^{+} cell fraction (0.34 ± 0.04 mM) indicating a clearly reduced mineralization potential of this subpopulation.

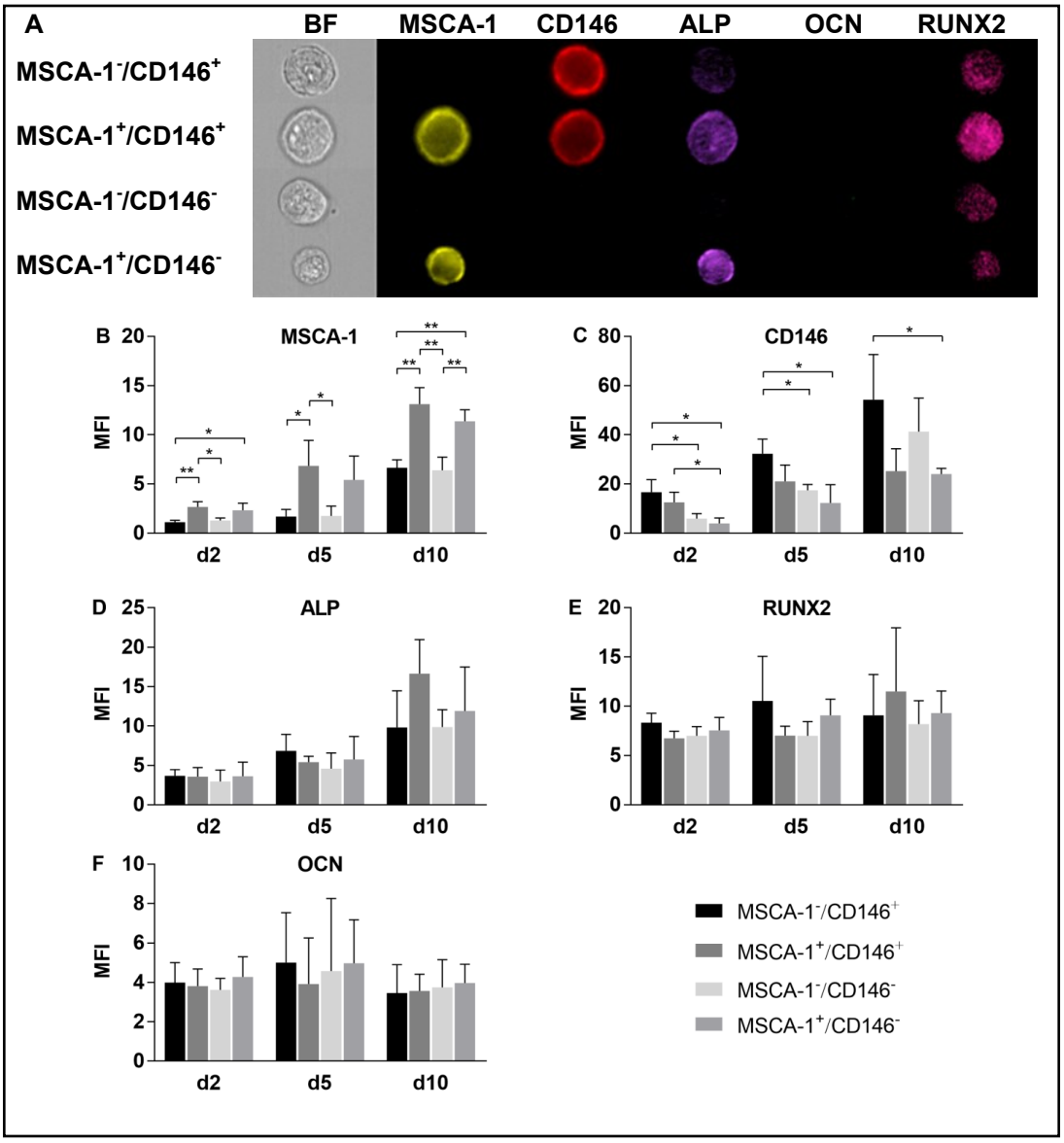

Fig. 5. A: Representative images of MSCA-1$^{+/-}$/CD146$^{+/-}$ separated cells analyzed by multispectral imaging flow cytometry after 5 days of osteogenic differentiation. Cells were labeled simultaneously with (yellow) anti-MSCA-1-PE, (red) anti-CD146-APC, (purple) anti-ALP + anti-IgG1-DyLight405 (permeabilized), (magenta) anti-RUNX2 + anti-IgG2a-PE-Cy7 (permeabilized) and (green) anti-OCN-AlexaFluor488 (permeabilized) antibodies. Lower panel: Median fluorescence indices (MFI) of FACS sorted MSCA-1$^{+/-}$/CD146$^{+/-}$ subpopulations after 2, 5 and 10 days of osteogenic differentiation, labeled with (B) anti-MSCA-1-PE, (C) anti-CD146-APC, (D) anti-ALP + anti-IgG1-DyLight405 (permeabilized), (E) anti-RUNX2 + anti-IgG2a-PE-Cy7 (permeabilized) and (F) anti-OCN-AlexaFluor488 (permeabilized) antibodies (n=3, * p<0.05).

Intra- and extracellular marker expression analysis by imaging flow cytometry

Osteogenic marker expression of FACS separated MSCA-1$^{+/-}$/CD146$^{+/-}$ subpopulations was analyzed after 2, 5 and 10 days of osteogenic differentiation (n = 3) by multispectral imaging flow cytometry (Fig. 5A). Coexpression of five different markers (MSCA-1, ALP, CD146, OCN, RUNX2) was analyzed and median fluorescence index (MFI) values were calculated (Fig. 5B-F). As expected, MFI values of MSCA-1 labeled subpopulations (Fig. 5B) (cell surface) were significantly higher in the two MSCA-1^{+} sorted subpopulations at day 2 of osteogenic induction. During the course of osteogenic differentiation, MSCA-1 expression

increased in all separated subpopulations, but remained significantly higher in the MSCA-1^+/$CD146^+$ and MSCA-1^+/$CD146^-$ subpopulation. This result correlates with the above mentioned higher mineralization potential of MSCA-1^+ sorted subpopulations, observed after 13 and 28 days of osteogenic differentiation (Fig. 4).

Fig. 5C illustrates MFI values of CD146 (surface labeling) labeled, MSCA-$1^{+/-}$/$CD146^{+/-}$ sorted subpopulations. MFI values were significantly higher in the two $CD146^+$ sorted subpopulations at day 2 of osteogenic induction. Similar to MSCA-1, CD146 expression increased in all subpopulations during the differentiation period. While CD146 expression strongly increased in both MSCA-1^- sorted subpopulations until day 10, the surface expression remained clearly lower in the two MSCA-1^+ sorted subpopulations.

Intracellular ALP expression (Fig. 5D) shows a similar pattern as MSCA-1 surface expression. After 2 and 5 days of differentiation, only minor differences in ALP expression were detectable between the four subpopulations. Until day 10, the expression increases in all subpopulations and is higher in the MSCA-1^+ sorted subpopulations, however without reaching statistical significance.

No significant differences could be detected concerning RUNX2 expression (Fig. 5E) during the experiment. Only at day 10, RUNX2 expression was slightly higher in MSCA-1^+ sorted subpopulations, revealing highest expression levels in the double positive population. These results are probably caused by an unspecific binding of the RUNX2 antibody resulting in a very high background signal.

Fig. 5F illustrates MFI values of OCN (intracellular labeling) labeled subpopulations. MFI values do not show any significant differences between the sorted subpopulations.

Quantitative gene expression analysis of ALP and RUNX2

Gene expression analysis was performed using a LightCycler instrument. Transcript levels were normalized to those of the housekeeping gene glycerinaldehyde 3-phosphate dehydrogenase (*GAPDH*), and illustrated in Fig. 6 as a ratio of the target versus the housekeeping gene transcripts.

As already detected on protein level by imaging flow cytometry, Fig. 6A shows increasing *ALP* gene expression during the osteogenic differentiation in all samples. Similarly, the two MSCA-1^+ subpopulations showed clearly higher expression levels than the MSCA-1^- subpopulations at the 3 time points analyzed.

RUNX2 gene expression was higher in both MSCA-1^+ subpopulations compared to the two MSCA-1^- subpopulations throughout the differentiation period, with the most significant differences detected at day 5 (Fig. 6B).

These results correlate with the previously shown mineralization pattern and the marker expression of the four sorted subpopulations.

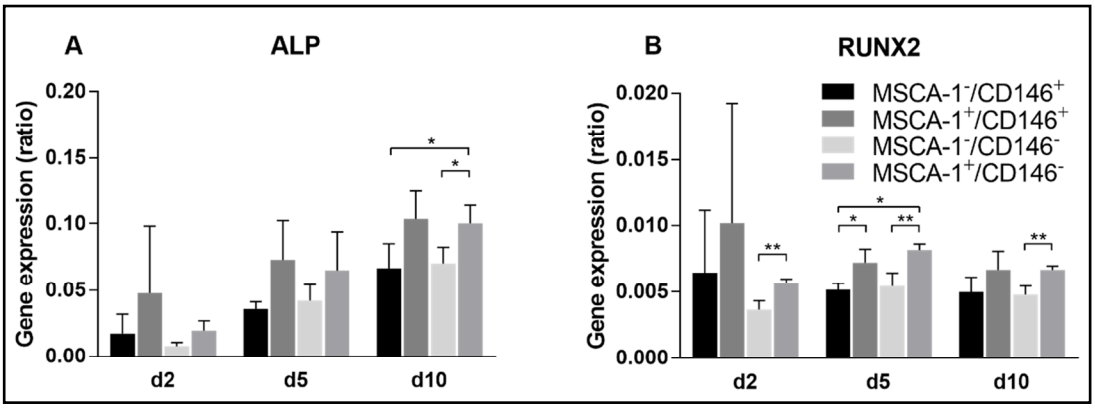

Fig. 6. A) ALP and B) RUNX2 gene expression (ratio of the target versus housekeeping (GAPDH) gene transcripts) in FACS sorted MSCA-$1^{+/-}$, $CD146^{+/-}$ subpopulations after 2, 5 and 10 days of osteogenic differentiation (n = 3, * $p \leq 0.05$).

Discussion

In the present study, we analyzed the osteogenic potential of MACS and FACS separated MSCA-$1^{+/-}$ and $CD146^{+/-}$ cell fractions isolated from an immortalized cranial periosteal cell line. As a result, we found a higher osteogenic potential in MACS separated MSCA-1^{+} and $CD146^{-}$ cell fractions in comparison to the opposite subpopulations.

The finding regarding the osteogenic potential of the MSCA-1^{+} subpopulation was expected based on our previous observation from human jaw periosteal cells [3]. The result concerning the osteogenic potential of the $CD146^{-}$ subpopulation was quite surprising due to the detection of significantly higher CD146 expression and osteogenic potential at the same time in TAg cells when compared to the originating primary cells [4]. Thus, we had hypothesized a positive correlation of CD146 expression and cell mineralization but found the opposite.

FACS separation provided a much more efficient and accurate separation of MSCA-1 and CD146 labeled cells compared to MACS separation. The low efficiency of magnetic CD146 separation was also described in the current work of Harkness and co-authors [22]. They also obtained significantly higher efficiencies of CD146 enrichment from a mesenchymal stem cell line overexpressing a human telomerase, using FACS in comparison to MACS separation.

In addition, FACS permits the separation of all four MSCA-$1^{+/-}$/$CD146^{+/-}$ subpopulations at the same time and is therefore more suitable for a closer look at the MSCA-$1^{+/-}$ and $CD146^{+/-}$ fractions.

Osteogenic differentiation of FACS separated TAg cells confirmed the reliability of MSCA-1 as a positive marker for osteogenic differentiation. Both, the MSCA-1^{+}/$CD146^{-}$ and the doubled-positive MSCA-1^{+}/$CD146^{+}$ subpopulation showed a strong calcium phosphate precipitation and a high expression of osteogenic markers.

MSCA-1 is known to be identical to the tissue non-specific alkaline phosphatase (ALP) [7], which plays an essential role in bone mineralization [23]. Based on this knowledge it is not surprising to find a high expression of MSCA-1 on MSCs committed to the osteogenic lineage.

In contrast, the function in bone mineralization of CD146, corresponding to the melanoma cell adhesion molecule (MCAM), is unknown. Ulrich et al. previously reported a higher osteogenic potential of MACS separated $CD146^{+}$ placenta-derived MSCs [24], however our results with MSCs from cranial periosteum showed the direct opposite. MACS separation led in our study to a negative correlation between CD146 expression and mineralization.

FACS separation into the four MSCA-$1^{+/-}$/$CD146^{+/-}$ subpopulations and subsequent imaging flow cytometry analysis revealed a more complex pattern of CD146 expression. On the one hand, we observed a significantly lower mineralization potential of the MSCA-1^{-}/$CD146^{+}$ subpopulation, compared to all other fractions. On the other hand, we detected a high mineralization potential in the double-positive MSCA-1^{+}/$CD146^{+}$ fraction. Here, the negative correlation of CD146 expression and mineralization was presumably masked by the effect of MSCA-1 expression, since a negative correlation between CD146 expression and mineralization remains when considering the MSCA-1^{+} and MSCA-1^{-} cells separately. Thus, we assume that CD146 plays only an indirect role during osteogenic differentiation.

In TAg cells, higher expression levels of both surface markers and a stronger mineralization potential were detected compared to the parental cells [4]. However, the present data indicates that CD146 expression does not play a key role for the osteogenic differentiation of cranial periosteal cells. Moreover, strong CD146 expression is probably a concomitant phenomenon in TAg cells or is related to the pericytic origin of the immortalized cells.

One possible explanation for lower mineralization potential in $CD146^{+}$ cells is that CD146 defines a subset of CPCs which is committed to a non-osteogenic lineage. Espagnolle et al., for example, describe CD146 to be a marker for vascular smooth muscle cell commitment of bone marrow MSCs [25].

Another explanation could be a more naïve differentiation state of $CD146^+$ cells. Similar to our *in vitro* results, Harkness et al. reported that bone formation was significantly enhanced in subcutaneous implants containing $CD146^-$ cells, indicating a higher osteogenic potential of this fraction [22]. They also detected a higher plasticity and the ability of transendothelial migration of $CD146^+$ cells, which suggests that $CD146^+$ cells are recruited to the bone surfaces by chemotactic attraction, and the subsequent maturation to osteoblasts goes hand in hand with the loss of CD146 expression. Inconsistent to this, we found an increase in CD146 expression in all subpopulations during osteogenic differentiation as well as in the controls. A plausible explanation could be an induction of CD146 expression stimulated by the increasing confluency during the differentiation period. MCAM (CD146) is known to play a role in cell adhesion and cohesion [26] and a similar correlation between CD146 expression and cell density in HUVECs has been reported by Bardin et al. [27].

Conclusion

Taken together, we assume that the high CD146 expression in our TAg cells does not correlate with a high osteogenic potential, but is rather related to the immortalization, conferring migratory properties upon the TAg cells. However, we did not test this feature in the present study. Similarly to the herein examined TAg cells, SV40 T-antigen immortalized endothelial progenitor cells (EPCs) from human cord blood were shown to be strongly positive for CD146 [28], as well as hTERT immortalized EPCs [29]. A recent study describes CD146 expression in mouse $p19^{ARF-/-}$, which show longer tumor latency as $p53^{-/-}$ mice [30]. Loss of $p19^{ARF}$ is supposed to overcome senescence and allow infinite proliferation without gaining malignant properties.

We conclude, that the $MSCA\text{-}1^+$ subpopulation isolated from the human cranial periosteal cell line represents a subpopulation with higher osteogenic potential compared to the opposite fraction. Hence, the elevated MSCA-1 expression in the immortalized TAg cell line indicates it's higher osteogenic potential compared to the parental cells.

In contrast to MSCA-1, the elevated CD146 expression of the TAg cell line is primarily an osteogenesis independent phenomenon, which might be associated with the immortalization process.

Acknowledgements

This work was supported in part by a grant from the Ministry of Science, Research and Arts of Baden-Württemberg (Az.: SI-BW 01222-91) and the Deutsche Forschungsgemeinschaft DFG (German Research Foundation) (Az.: INST 2388/33-1).The works included in this study were approved by the local ethics committee (approval number 534/2013BO1).

Disclosure Statement

The authors of this publication declare no conflicts of interest.

References

1 Ferretti C, Mattioli-Belmonte M: Periosteum derived stem cells for regenerative medicine proposals: Boosting current knowledge. World J Stem Cells 2014;6:266-277.

2 Ceccarelli G, Graziano A, Benedetti L, Imbriani M, Romano F, Ferrarotti F, Aimetti M, Cusella de Angelis GM: Osteogenic Potential of Human Oral-Periosteal Cells (PCs) Isolated From Different Oral Origin: An *In vitro* Study. J Cell Physiol 2016;231:607-612.

3 Alexander D, Schafer F, Olbrich M, Friedrich B, Buhring HJ, Hoffmann J, Reinert S: MSCA-1/TNAP selection of human jaw periosteal cells improves their mineralization capacity. Cell Physiol Biochem 2010;26:1073-1080.
4 Alexander D, Biller R, Rieger M, Ardjomandi N, Reinert S: Phenotypic characterization of a human immortalized cranial periosteal cell line. Cell Physiol Biochem 2015;35:2244-2254.
5 Frenette PS, Pinho S, Lucas D, Scheiermann C: Mesenchymal Stem Cell: Keystone of the Hematopoietic Stem Cell Niche and a Stepping-Stone for Regenerative Medicine. Annual Review of Immunology 2013;31:285-316.
6 Dominici M, Le Blanc K, Mueller I, Slaper-Cortenbach I, Marini F, Krause D, Deans R, Keating A, Prockop D, Horwitz E: Minimal criteria for defining multipotent mesenchymal stromal cells. The International Society for Cellular Therapy position statement. Cytotherapy 2006;8:315-317.
7 Sobiesiak M, Sivasubramaniyan K, Hermann C, Tan C, Örgel M, Treml S, Cerabona F, de Zwart P, Ochs U, Müller CA, Gargett CE, Kalbacher H, Bühring H-J: The Mesenchymal Stem Cell Antigen MSCA-1 is Identical to Tissue Non-specific Alkaline Phosphatase. Stem Cells Dev 2009;19:669-677.
8 Devito L, Badraiq H, Galleu A, Taheem DK, Codognotto S, Siow R, Khalaf Y, Briley A, Shennan A, Poston L, McGrath J, Gentleman E, Dazzi F, Ilic D: Wharton's jelly mesenchymal stromal/stem cells derived under chemically defined animal product-free low oxygen conditions are rich in MSCA-1(+) subpopulation. Regen Med 2014;9:723-732.
9 Noort WA, Oerlemans MI, Rozemuller H, Feyen D, Jaksani S, Stecher D, Naaijkens B, Martens AC, Buhring HJ, Doevendans PA, Sluijter JP: Human versus porcine mesenchymal stromal cells: phenotype, differentiation potential, immunomodulation and cardiac improvement after transplantation. J Cell Mol Med 2012;16:1827-1839.
10 Esteve D, Boulet N, Volat F, Zakaroff-Girard A, Ledoux S, Coupaye M, Decaunes P, Belles C, Gaits-Iacovoni F, Iacovoni JS, Remaury A, Castel B, Ferrara P, Heymes C, Lafontan M, Bouloumie A, Galitzky J: Human white and brite adipogenesis is supported by MSCA1 and is impaired by immune cells. Stem Cells 2015;33:1277-1291.
11 Buhring HJ, Treml S, Cerabona F, de Zwart P, Kanz L, Sobiesiak M: Phenotypic characterization of distinct human bone marrow-derived MSC subsets. Ann N Y Acad Sci 2009;1176:124-134.
12 Battula VL, Treml S, Bareiss PM, Gieseke F, Roelofs H, de Zwart P, Muller I, Schewe B, Skutella T, Fibbe WE, Kanz L, Buhring HJ: Isolation of functionally distinct mesenchymal stem cell subsets using antibodies against CD56, CD271, and mesenchymal stem cell antigen-1. Haematologica 2009;94:173-184.
13 Hofmann C, Liese J, Schwarz T, Kunzmann S, Wirbelauer J, Nowak J, Hamann J, Girschick H, Graser S, Dietz K, Zeck S, Jakob F, Mentrup B: Compound heterozygosity of two functional null mutations in the ALPL gene associated with deleterious neurological outcome in an infant with hypophosphatasia. Bone 2013;55:150-157.
14 Whyte MP: Physiological role of alkaline phosphatase explored in hypophosphatasia. Ann N Y Acad Sci 2010;1192:190-200.
15 Orimo H: The mechanism of mineralization and the role of alkaline phosphatase in health and disease. J Nippon Med Sch 2010;77:4-12.
16 Matsuura S, Kishi F, Kajii T: Characterization of a 5'-flanking region of the human liver/bone/kidney alkaline phosphatase gene: two kinds of mRNA from a single gene. Biochem Biophys Res Commun 1990;168:993-1000.
17 Esteve D, Galitzky J, Bouloumie A, Fonta C, Buchet R, Magne D: Multiple Functions of MSCA-1/TNAP in Adult Mesenchymal Progenitor/Stromal Cells. Stem Cells Int 2016;2016:1815982.
18 Stark K, Eckart A, Haidari S, Tirniceriu A, Lorenz M, von Bruhl ML, Gartner F, Khandoga AG, Legate KR, Pless R, Hepper I, Lauber K, Walzog B, Massberg S: Capillary and arteriolar pericytes attract innate leukocytes exiting through venules and 'instruct' them with pattern-recognition and motility programs. Nat Immunol 2013;14:41-51.
19 Crisan M, Yap S, Casteilla L, Chen CW, Corselli M, Park TS, Andriolo G, Sun B, Zheng B, Zhang L, Norotte C, Teng PN, Traas J, Schugar R, Deasy BM, Badylak S, Buhring HJ, Giacobino JP, Lazzari L, Huard J, Peault B: A perivascular origin for mesenchymal stem cells in multiple human organs. Cell Stem Cell 2008;3:301-313.
20 Bianco P, Sacchetti B, Riminucci M: Osteoprogenitors and the hematopoietic microenvironment. Best Pract Res Clin Haematol 2011;24:37-47.

21 Olbrich M, Rieger M, Reinert S, Alexander D: Isolation of Osteoprogenitors from Human Jaw Periosteal Cells: A Comparison of Two Magnetic Separation Methods. PLoS One 2012;7:e47176.
22 Harkness L, Zaher W, Ditzel N, Isa A, Kassem M: CD146/MCAM defines functionality of human bone marrow stromal stem cell populations. Stem Cell Res Ther 2016;7:4.
23 Sapir-Koren R, Livshits G: Bone mineralization and regulation of phosphate homeostasis. IBMS BoneKEy 2011;8:286-300.
24 Ulrich C, Abruzzese T, Maerz JK, Ruh M, Amend B, Benz K, Rolauffs B, Abele H, Hart ML, Aicher WK: Human Placenta-Derived CD146-Positive Mesenchymal Stromal Cells Display a Distinct Osteogenic Differentiation Potential. Stem Cells Dev 2015;24:1558-1569.
25 Espagnolle N, Guilloton F, Deschaseaux F, Gadelorge M, Sensébé L, Bourin P: CD146 expression on mesenchymal stem cells is associated with their vascular smooth muscle commitment. J Cell Mol Med 2014;18:104-114.
26 Wang Z, Yan X: CD146, a multi-functional molecule beyond adhesion. Cancer Lett 2013;330:150-162.
27 Bardin N, Anfosso F, Massé J-M, Cramer E, Sabatier F, Bivic AL, Sampol J, Dignat-George F: Identification of CD146 as a component of the endothelial junction involved in the control of cell-cell cohesion. Blood 2001;98:3677-3684.
28 Qiu HY, Fujimori Y, Nishioka K, Yamaguchi N, Hashimoto-Tamaoki T, Sugihara A, Terada N, Nagaya N, Kanda M, Kobayashi N, Tanaka N, Westerman KA, Leboulch P, Hara H: Postnatal neovascularization by endothelial progenitor cells immortalized with the simian virus 40T antigen gene. Int J Oncol 2006;28:815-821.
29 Paprocka M, Krawczenko A, Dus D, Kantor A, Carreau A, Grillon C, Kieda C: CD133 positive progenitor endothelial cell lines from human cord blood. Cytometry A 2011;79:594-602.
30 Koudelkova P, Weber G, Mikulits W: Liver Sinusoidal Endothelial Cells Escape Senescence by Loss of p19ARF. PLoS One 2015;10:e0142134.